Nanofaceting of vicinal Nb(011)

C. P. Flynn, W. Swieçh, R. S. Appleton, and M. Ondrejcek*
Frederick Seitz Materials Research Laboratory, University of Illinois at Urbana Champaign, Urbana, Illinois, 61801
(Received 16 November 1999; revised manuscript received 28 January 2000)

We report studies of vicinal Nb(011) grown heteroepitaxially on sapphire $(11\bar{2}0)$. Using low-energy electron microscopy on surfaces with small vicinal miscut ~0.1°, we record the evolution of step edges during annealing in ultrahigh vacuum. Below a temperature of about 1600 K the step edges coalesce to form {110} nanofacets several steps in height, due to the low surface free energy. Two distinct types of facet form, depending on the direction of miscut. For miscut along $[0\bar{1}1]$,$(01\bar{1})$ facets, which intersect the (011) terraces at 90° along [100], are created by step-edge coalescence. Owing to $(2mm)$ symmetry, these occur over a range of orientations around [100]. The surface develops over the course of hours into large terraces more than 10 μm long and of widths up to several μm, terminated by $(01\bar{1})$ facets tens of atomic (011) planes in height. Surfaces miscut instead along [100] develop $(\bar{1}10)$ facets at 60° to the (011) terraces, which they intersect along $[\bar{1}\bar{1}1]$ and $[\bar{1}1\bar{1}]$, respectively. The surface ripens into long terraces bounded by serrated edges formed from alternating nanofacets about five steps in height. A variety of interesting phenomena are observed, including direct nucleation of nanofacets from step edges, growth in a sawtooth of alternating facets, and periodically faceted states in which facet sections alternate with sections in which the step edges are dissociated, to make a periodic structure. The phase diagram for nanofaceting is discussed for the limit of small miscut.

I. INTRODUCTION

Nanotopographical features of surfaces have attracted interest in the recent literature. One example is hut structures induced by strain in epitaxial Si-Ge alloys.[1,2] A second example is the careful study of facets on bulk crystals in thermal equilibrium.[3,4] The faceting behavior of crystals grown by epitaxy is not yet well understood. For example, it is not yet possible to calculate phase diagrams that predict the facet structures as functions of temperature and vicinal miscut.[5,6] This is in contradistinction to the case for bulk crystals where the answer is available, in principle, from the Wulff[7] construction, given that the surface free energy is a known function of orientation. Symmetry factors that influence the shapes of macroscopic crystals grown off-equilibrium from solution or the vapor phase are likewise well documented.[8] The present work concerns the nanofacets that occur as a function of temperature on the surface of a metal, Nb, grown heteroepitaxially on an insulating substrate of sapphire (Al_2O_3). These facets are typically five atomic planes or about 1 nm high.[9] Niobium is of special interest as a metal known to facet easily on {110} planes, and the heteroepitaxy of Nb(011) on sapphire $(11\bar{2}0)$ has been studied. These matters are documented further in what follows.

Owing to their thin-film geometry, faceting of heteroepitaxial systems differs from the behavior of bulk samples. Because the diffusion time required for a significant redistribution of material over the surface is inaccessibly long, realizable experimental conditions are restricted to a subset of configurations in which the film remains essentially uniform in thickness. This means that the surface orientation, when averaged over a suitable locality, remains a fixed quantity. For a vicinal crystal the orientation may equally be regarded as the miscut from the nearby low-index plane. The actual surface configuration is specified by the distribution of atomic steps on the surface, or equivalently by the terraces that these step edges interconnect.[5,6] The constraint on the equilibrium of a thin film is therefore the condition that the local density and mean orientation of step edges remain fixed, when averaged over a suitable locality. Predictions of phase diagrams for faceting therefore require a statistical treatment of interacting step edges of density and orientation that correspond to the specified vicinal miscut. It is this problem that remains at present unsolved.

Much evidence bears on the observation that Nb facets readily on {110} surfaces. These are the six most closely packed planes of the bcc structure. A reservation here derives from experiments that show temperatures of 2600 K in UHV are needed to free the Nb(011) surface from oxygen contamination.[10,11] Most experimental studies, including those reported here, are therefore conducted with some surface oxygen present. For bcc metals it is common for {110} to be the planes of least surface free energy, but for Nb the energy is low relative to the melting temperature even in comparison to the remaining bcc metals.[12] A compilation of experimental surface energies, together with fitted model potentials and their predictions, is given in Ref. 12. In experiments that use Nb foils annealed at high temperatures, it is observed that large-scale faceting takes place, usually on {110} planes but also on {111} planes.[13] Surfaces of sufficient quality have been prepared by these means that foils 5 μm thick have provided suitable substrates for subsequent heteroepitaxial growth of single-crystal overlayers by molecular-beam epitaxy (hereafter abbreviated to MBE).[14]

In addition, Nb has been grown directly on sapphire by MBE,[15] both as a model system for investigation of metal-ceramic interfaces[16–18] and as a generally useful buffer layer to decouple subsequent overgrowths from sapphire single-

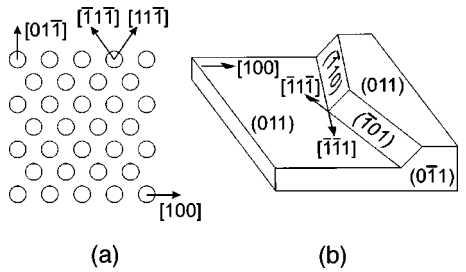

FIG. 1. (a) Atomic positions and principal directions in the bcc(011) plane. (b) Three types of facets that occur on the Nb(011) vicinal surface. The $(0\bar{1}1)$ facet is at 90° to the (011) surface, and intersects it along [100]. The two 60° facets are $(\bar{1}10)$ and $(\bar{1}01)$; they intersect (011) along $[\bar{1}\bar{1}1]$ and $[\bar{1}1\bar{1}]$, respectively. The 60° facets are shown for miscut (positive gradient) along [100]. There are three equivalent facets for other miscuts.

crystal substrates.[19–21] The latter are available commercially with epitaxial finish, and therefore provide a convenient starting point for heteroepitaxial synthesis.[22] Several orientations of sapphire substrate yield Nb so oriented that the two lattices retain a unique three-dimensional relationship among the several cases, due to bonding geometry at the atomic level.[23,16] Nb(011) grows best on sapphire $(11\bar{2}0)$ in the temperature range above 800 °C. A regime of temperature, thickness, and miscut exists in which samples grown by MBE develop mesostructures with a typical length scale of 0.1–10 μm.[24] These mesostructures grow with precisely the {110}- faceted surfaces that are of interest in the present research.

Details of the relevant geometry will be useful for what follows. Figure 1(a) shows atomic positions on the bcc(011) surface and identifies certain crystallographic direction within the plane. In Fig. 1(b) are shown three {110} facet planes that intersect (110), namely, $(0\bar{1}1)$ at 90° to the surface, and $(\bar{1}10)$ and $(\bar{1}01)$ at 60°. They intersect (011) along the [100], $[\bar{1}\bar{1}1]$, and $[\bar{1}1\bar{1}]$ directions, respectively. These are the in-plane directions associated with facets of low energy. For vicinal Nb(011), the 60° cases appear for miscut (positive gradient) along [100], while the 90°$(0\bar{1}1)$ facet appears for $[01\bar{1}]$ miscut. A further three facets pertinent to (011) are $(01\bar{1})$ at 90° to the surface, for miscut along $[0\bar{1}1]$, and (101) and (110) at 60° for miscut along $[\bar{1}00]$. These three intersect with (011) along the same directions as the first three.

In the present research, facets are detected mainly by low-energy electron microscopy and scanning tunneling microscopy, shortened in what follows to LEEM and STM. A summary of initial results on a Nb(011) surface is available,[25] and the observation of periodically faceted states on Nb(011) miscut along [100] has been reported.[9] A brief account of experimental MBE, LEEM, and STM matters is given in Sec. II. The experimental results, together with a discussion of their significance, are presented in Sec. III. A phase diagram for nanofacetting is described in Sec. IV, and conclusions drawn from the research are the subject matter of Sec. V.

II. EXPERIMENTAL MATTERS

Specimens were prepared by molecular-beam epitaxy, and examined by low energy electron microscopy. Summaries of the relevant processes are provided here.

A. Film growth

In all, five Nb thin-film samples were grown and examined in this work. Three, of thicknesses 160, 160, and 50 nm, were grown on sapphire miscut to give the resulting Nb(011) surface a vicinal tilt of about 0.1° along Nb$[0\bar{1}1]$. The remaining two, with thicknesses of 227 and 500 nm, were grown with a vicinal tilt of about 0.1° along [100]. In each case commercial sapphire substrates[22] with epitaxial grade polish were degreased and passed through ultrasonic cleaning baths, before being dried and introduced into the growth chamber. There the substrates were subject to an annealing procedure to condition the sapphire surface. The Nb films were then grown at about 1170 K with a rate of ~0.2 A/s, until the desired thickness was achieved. For more details of these now standard procedures, the reader should consult Refs. 15 and 19–21. A number of the samples were subsequently stored in a low vacuum dessicator and in air before being introduced into the LEEM for analysis.

B. LEEM studies

The electron microscope employed in this research was designed by Tromp, following the work of Bauer,[26] and was constructed at IBM Yorktown Heights. A description of the design will be found in the literature.[27] The LEEM permits research on surfaces, at a lateral resolution of ~10 nm, to be conducted at a base pressure of 1×10^{-10} torr. Dark and bright-field imaging modes are both available, as is surface diffraction by low-electron electron diffraction (LEED). In addition, a sample stage and electron-beam heating equipment have been incorporated to permit the study of metals grown on insulating substrates at temperatures up to 1720 K. Different samples afforded diverse periods of study, as the heater design was perfected over the course of this research.[25] Early samples cracked, owing to inhomogeneous heating and from exposure to the electron-beam heater. With later designs, one sample 500 nm thick miscut along [100] seemed to offer an indefinitely long life, and was finally destroyed by experiments that exposed it deliberately to air oxidation at high temperature, from which condition it was not possible to restore a ''clean''state.

In the present research, it was found that the Nb surface cleaned to yield a nearly perfect 1×1 LEED pattern above 1500 K, after cycling up to 1720 K in a vacuum never worse than about 3×10^{-9} torr. In this, Nb(011) resembles Mo(011), for which the cleaning cycle was reported elsewhere.[28] Earlier results of other researchers established, however, that the Nb surface remains oxygen doped unless heated in UHV to much higher temperatures of ~2600 K, which were not available in LEEM.[10,11] Consequently the surfaces studied here undoubtedly retained some oxygen coverage despite the 1×1 LEED pattern. The same thermal cycling that cleaned off surface phases simultaneously permitted dislocation motion and greatly improved the crystalline quality of the Nb films.[28] Details of the transformation

of the films and their surfaces under thermal cycling are not relevant to the faceting behavior described here, and will be reported elsewhere. The results presented in Sec. III were taken using materials in which the cleaning process is well advanced. Some results nevertheless relate to the interaction of dislocations with facets. These concerned residual dislocations in crystals for which the thermal processing remained incomplete.

C. STM studies

Scanning tunnelling microscopy has also been employed to examine Nb single-crystal films, using an Omicron variable temperature STM, further equipped with LEED with four-grid electron optics and a cylindrical mass analyzer for Auger spectroscopy. 500-nm Nb films miscut by about 0.1° along [100] were prepared by MBE, as detailed above, and heated to 1670 K by a current passed through about a 1-μm thickness of Nb or Ta which was magnetron sputtered on the rear surface of the sapphire substrate. After extensive outgassing at 850 K, the Nb surfaces were cleaned by heating for several hours to 1500 K, followed by flashes to 1670 K, following procedures similar to those employed in the LEEM studies. When checked by Auger and LEED spectroscopies, the surfaces showed no trace of impurities other than oxygen, with almost constant O_{KKL} (510 eV) to Nb ratio observed up to 1570 K. Two variants of surface reconstruction observed by LEED at 300 K agreed well with those observed in LEEM.[25] The Nb thin layer degraded over the course of days to form a rough surface, and fingering of the type reported earlier[24] occurred, perhaps owing to electromigration caused by the heating current.[29]

III. RESULTS

LEEM observations were made on Nb(011) surfaces with weak miscut, ~0.1° relative to (011). In all cases the surfaces had first been cycled to high temperature in a vacuum of 3×10^{-9} torr at worst, until surface deposits (mainly carbon traces) were no longer visible, and LEED at 1500 K revealed only a 1×1 surface structure. The intermediate structures that occur as Nb(011) passes from a MBE-grown but air-exposed state to the cleaned but still oxygen-covered from (see above) are of separate interest, and will be reported elsewhere.

The results identify three categories of structure. At the highest temperatures is a regime in which steps are mainly dissociated, so that the surface is covered mostly by single-height step edges. At low temperatures is a regime in which nanofacets, rather than single steps, accommodate the Nb(011) miscut. These occur during annealing as the surface structure ripens. In our observations the nanofacets range from 3 to ~20 atomic planes high, or about 1–4 nm. Finally, and most complicated, are intermediate regimes in which both nanofacets and single step edges occur on the surface, either in quasiequilibrium configurations or as configurations passed through during the kinetics of transformation between stepped and faceted surfaces. In what follows, LEEM images are employed to investigate the structures of these surfaces and the mechanisms by which transformations take place among them.

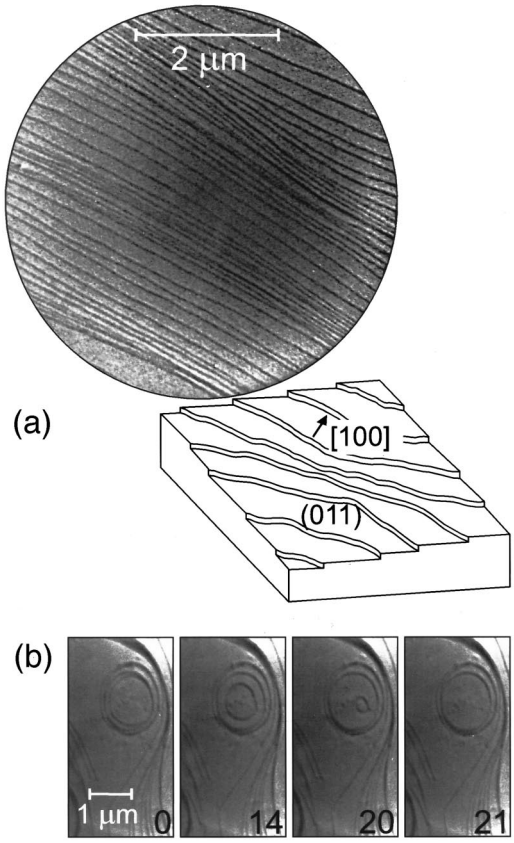

FIG. 2. LEEM images of Nb(011) in the single step regime at high temperatures. (a) Nb(011) miscut by 0.1° along [100] taken with $E_p=9$ eV at 1720 K. (b) Images showing loop shrinking during annealing at 1590 K, taken with $E_p=11$ eV. The numbers give the time in seconds. The loop has a round shape, showing that the energy of the steps is fairly isotropic.

A. High temperatures: Surfaces with mainly single steps

In equilibrium at the highest temperatures employed in the present studies, miscut of the Nb(011) surface is accommodated almost entirely by step edges of unit height. Moreover, the characteristics of the steps appear to be relatively isotropic. The general type of stepped structure is illustrated by a sketch shown in Fig. 2, where single steps are separated by terraces of variable width that, in the case illustrated, correspond to a miscut generally along the [100] azimuth. All samples studied here, regardless of thickness and orientation of miscut, had surfaces that cleaned and annealed to form this type of structure at a temperature near 1670 K.

The observed high-temperature surfaces are exemplified by the micrographs in Fig. 2(a). The precise contrast with which the steps are imaged depends on diffraction conditions, and hence on the impact energy E_p of the primary electron beam. For this reason the beam energy is included throughout the paper as information provided in the figure captions. Figure 2(a) shows a fairly ideal surface at 1720 K, miscut by about 0.1° along [100], comparable in fact to those observed in LEEM studies of Mo(011).[28] One distinction is that for Mo the oxygen is largely removed at 1670 K.

Inspection of the stepped surfaces reveals that the step edges are fairly straight, with separations that do not change much on the length scale of their average spacing. In addition, the spacings often appear to be more uniform than

would be anticipated of a random system. These behaviors relate to the stiffness of step edges and the interactions among them. Observations of spatial and temporal step fluctuations can quantify these factors,[30] and it is our intention to present a detailed analysis of the phenomena in a separate paper.

Since Nb(011) has tetragonal ($2mm$) symmetry,[31] surface steps must generally exhibit anisotropic characteristics. At a microscopic level the close packed step edges (see Fig. 1) lie along $[\bar{1}1\bar{1}]$ and $[\bar{1}\bar{1}1]$, and steps oriented along [100] have edge atoms spaced as second-nearest neighbors. Regardless of this anisotropic geometry, the observed behavior of step edges on Nb(011) is fairly isotropic. To illustrate this, Fig. 2(b) shows a sequence of images, from an early stage of annealing, in which step loops shrink and eventually vanish as diffusion over the surface gradually fills in a surface depression. The loops remain rather circular in shape (despite pinning at visible edge dislocations that thread the sample), whereas a strong anisotropy of the line energy would certainly make the quasi-equilibrium loop shape anisotropic. This is observed, for example, on Si(001),[32] which also has ($2mm$) symmetry. Here the possible anisotropy of the loops is ~20%, thus reflecting similar limits in the anisotropy in the line tensions of step edges.

B. Low temperatures: Faceted surfaces

The faceted surfaces that occur on weakly miscut Nb(011) at temperatures below about 1650 K depend on the direction of miscut. We have investigated two cases with orthogonal miscuts along [100] and $[0\bar{1}1]$, respectively.

$[0\bar{1}1]$ *miscut*. During annealing of a rough (011) Nb surface at temperatures of 1550–1720 K, step edges bunch to appear in LEEM as notably straight lines along three crystallographic directions. Figure 3(a) provides the example of a Nb film 160 nm thick. The close, packed $[\bar{1}1\bar{1}]$ and $[1\bar{1}1]$ directions both appear, together with [100]. We interpret the lines in the LEEM image as facets of the type identified in Fig. 1. The surface, as shown, is at 1620 K and far from equilibrium; all three types of facet are observed together only in initial heating cycles. It is interesting that the close-packed facet directions develop first, even though the miscut could be accommodated by steps mainly along [100]. This interpretation is encouraged but not firmly established by the LEEM images alone, owing to the limited lateral resolution ~10 nm.

In addition, following earlier results[33] we have been able to image the Nb(011) surface by scanning tunneling microscopy. Figure 3(b) and insets show facets as observed by STM. The upper image scans wide terraces with abrupt facets many steps high, and in addition a single height step (see the inset line scan). We have made an attempt to determine how steep the facets appear in STM. The lower image shows a close-packed facet five steps high, as revealed both by its height of 1.1 nm and the separate steps visible at the jog. In the STM image inset the height change occurs over a distance of about 2 nm. This establishes unambiguously that the feature is too narrow to comprise five dissociated steps separated by atomic displacements, and indeed a configuration of several steps, each oriented crystallographically and spaced by one or two atomic displacements, does not appear to make physical sense unless they form a specific facet of low energy. We conclude that the inference from LEEM that the lines in Fig. 3(a) correspond to nanofacets is consistent also with the STM evidence. Further work is needed to make the identification unambiguous. In what follows these features are identified as nanofacets of the types depicted in Fig. 1, although this remains an inference.

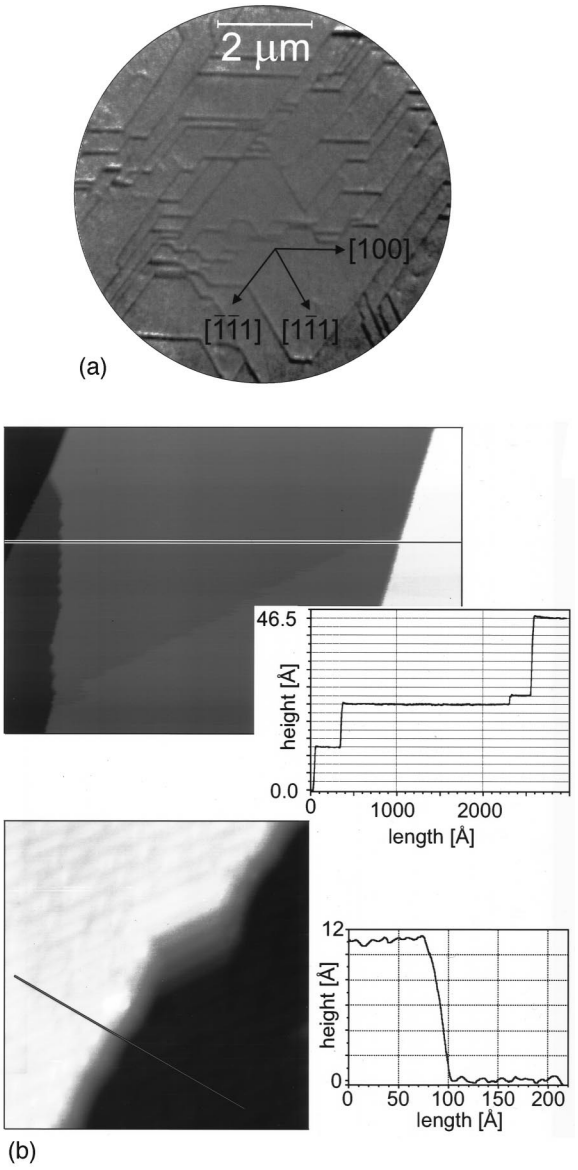

FIG. 3. Nanofacets. Part (a) shows a rough Nb(011) surface miscut along $[0\bar{1}1]$, and partly annealed to create terraces up to ~1 μm wide. The straight lines along [100], $[\bar{1}1\bar{1}]$, and $[1\bar{1}1]$ that terminate the terraces are interpreted as nanofacets. The image is acquired at $T=1620$ K and $E_p=9$ eV. In the STM images of (b), the upper figure shows a long terrace terminated at each end of the identified line scan (shown inset) by steep facets. The terrace contains a single step edge which moves, and thus forms an irregular separating line between two different grays. In the lower image the facet is 1.1 nm high and breaks into five separate steps at the jog. The inset shows that the height change occurs with maximum slope >0.5 or ~30°, even when reduced by tip size effects. It is inferred that the steps have merged to form a single crystallographic facet. This is a nonequilibrium configuration from an early annealing cycle.

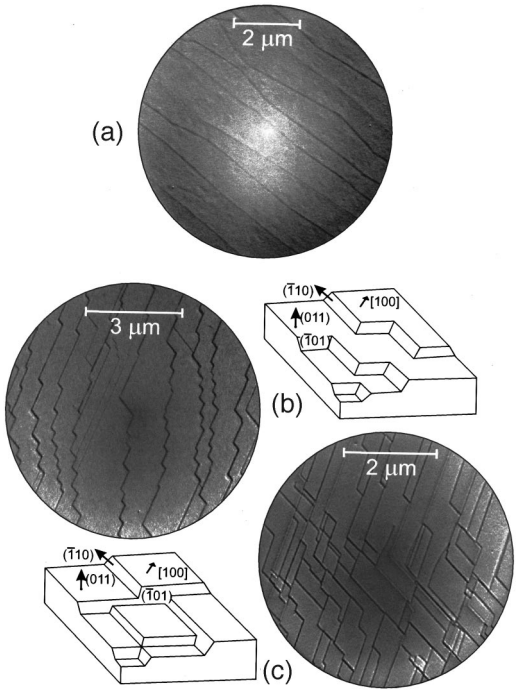

FIG. 4. Nanofacets and steps. (a) Gently curving facets oriented generally near $(01\bar{1})$ and aligned close to [100] on a vicinal surface miscut along $[0\bar{1}1]$ and annealed at about 1560 K. (b) and (c) Surfaces miscut along [100] and annealed near 1410 and 1615 K, showing $(\bar{1}10)$ and $(\bar{1}01)$ nanofacets in two characteristic forms. In (b) the facets are short and cause the terraces to have serrated edges, while in (c) the facets are long and divide the (011) terraces, as shown in the inset sketches. Values of E_p for the three images are 6, 42, and 4 eV.

A smoother (011) surface, from a later stage of annealing, but still miscut along $[0\bar{1}1]$, reveals step edges mainly along [100]. This is not a close-packed direction but, as several [100] step edges accumulate along the same line, they can stack to form a single vertical nanofacets of $(01\bar{1})$ orientation. Because the {110} surfaces of Nb have low surface free energies, this stacking process is energetically favored, and the surface evolves into (011) terraces connected by long $(01\bar{1})$ facets. Over the course of time these surface features ripen. The image in Fig. 4(a) shows the surface of a film 50 nm thick, miscut by 0.1° along $[0\bar{1}1]$ and ripened for about 1 h at 1560 K. During this process single step edges can be seen to accumulate one by one at the facet (see below, Sec. III E). The terraces are ~1 μm wide and many μm long. We thus infer that the 90° $(01\bar{1})$ facets in these images are ~2 nm high or ~10 atomic (011) planes, so that they may properly be termed nanofacets.

It is interesting that the ripened nanofacets are not rigorously planar. While oriented generally along [100], they nevertheless curve among nearby orientations. Added annealing makes the facets higher and smoother (see Sec. III E). This suggests that the surface energy remains small for a range of surface orientations around $(01\bar{1})$. In turn this conclusion is consistent with the observation from the $(2mm)$ symmetry that the surface energy can change only in second order with the angle as any {110} plane is rotated from the exact [100] intersection. The proof is that the energy must by symmetry be the same for positive and negative rotations relative to each of the two mirror planes. It is conceivable that these 90° facets extend far enough to include 90° {111} facets, at 37° to the $(01\bar{1})$ pole.

[100] miscut. For this direction of miscut the close packed $[\bar{1}1\bar{1}]$ and $[1\bar{1}1]$ step edges are equally revealed, and no steps along [100] are needed. This leads to the prospect that $(\bar{1}10)$ and $(\bar{1}01)$ facets form when step edges coalesce. The micrographs in Figs. 4(b) and 4(c) for an epitaxial film 0.5 μm thick, annealed at 1410 and 1615 K, respectively, show that two different appearances of the surface can develop, respectively interpreted in their inset sketches. The sketches are again based on the inference that the observed straight lines, which are seen to follow the close packed crystallographic directions in Fig. 4, are in fact nanofacets. Typical facet heights observed in this work are 3–6 steps for [100] miscut and much more for $[0\bar{1}1]$ miscut. For a given facet height the difference between the two structures sketched in Fig. 4 lies in the length scale of the facets relative to their spacing along [100] (i.e., to their height for the given miscut). When the facets are short and high, the terraces remain long, and with the bounding edges serrated along the close-packed directions. When, on the other hand, the facets become long relative to the terrace width, they cross the entire terrace and the structure breaks into parallelograms with (011) terraces contained by $(\bar{1}10)$ and $(\bar{1}01)$ facets. Either way the surface achieves the low energy of an entirely {110} structure.

C. Mechanisms for nanofaceting of the [100] miscut surface

Mechanisms are required by which the surface can make transitions from one surface structure to the next as conditions change. For [100] miscut the availability of alternative facet orientations can lead to a complex surface evolution. In the course of these investigations we observed different pathways, some unexpected, by which the surface nucleates low energy facets.

Direct nucleation from interacting steps. When a surface with single step edges is cooled and held below the faceting temperature, nanofacets can be nucleated directly from the fluctuating step edges. One great advantage of LEEM is that processes can be followed in real time with a resolution of 33 ms. On this time scale the step-edge locations and profiles above 1470 K are seen to undergo large fluctuations. A series of micrographs in Fig. 5(a) shows how a nanofacet nucleates (black arrows) from an initially unbiased distribution of step edges with no nearby defects. Prior to visible nucleation, it is apparent in video sequences that several neighboring step edges fluctuate into an interacting group. A nucleus of the more favored facet then becomes visible in LEEM as a diagonal line crossing the steps. Later images show that the facet subsequently grows by coalescence of the step edges that dissociate from both its termini. Only limited growth of a single nanofacet has been observed, presumably because the angle between the steps and the facet tips becomes unfavorable as the length increases (for a relevant discussion, see Sec. III F below). What happens is that a second, better favored, facet is nucleated, as explained in what follows immediately.

Sawtooth faceting. We have observed that a nanofacet, once formed, can create a nanofacet sawtooth in which the

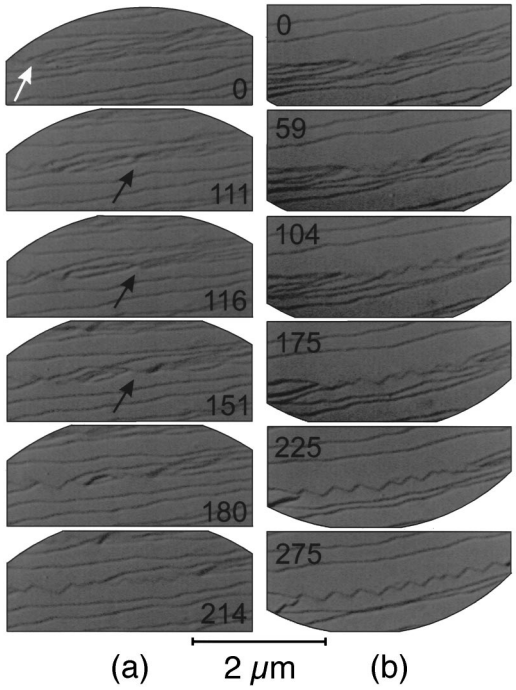

FIG. 5. Nucleation of 60° nanofacets. (a) The upper micrographs show a 60° nanofacet nucleating directly from fluctuating step edges at 1585 K, and further nucleating a sawtooth nanofacet. Image taken with $E_p = 4$ eV. (b) A sawtooth nanofacet forms and grows parallel to the dissociated steps (i.e. perpendicular to the local surface gradient) by nucleation of alternating facets in appropriate relative lengths from successive facet tips. The image is taken at $T = 1585$ K with $E_p = 4$ eV, chosen for visibility of single steps, so that the sawtooth has poor visibility. Numbers give time in seconds.

two {110} facet orientations alternate, maintaining the same set of step edges throughout. The series of facets runs along the same direction as the original step edges to accommodate the miscut perfectly. Evidently when the angles that step edges make with a facet terminus become unfavorable, the alternative orientation of facet can nucleate directly at the facet tip to continue the faceting process as a sawtooth. This process is initiated in the final two images of Fig. 5(a). The sequence of micrographs in Fig. 5(b) show how, for an epilayer 500 nm thick at a temperature of 1585 K, the sawtooth faceting can proceed for tens of nanofacets, extending for several microns, along the precise average orientation of the dissociated steps (i.e., along the normal to the miscut). A point of added interest is that the sawtooth shown contains precisely five step edges. For this step height the LEEM contrast is close to a minimum for the impact energy employed to optimize the visibility of single step edges. Consequently the visibility of the sawtooth facet in the micrograph is poor.

Dislocation drag. Dislocations are observed to exert forces on step edges. When an edge dislocation that intersects the surface glides through a field of step edges, it perturbs the steps in a way that is readily detected in LEEM images. By way of example, in Fig. 6(a) a gliding edge dislocation intersects a field of five single step edges about 0.5 μm from the point at which they coalesce to form a facet. The perturbation stretches the steps almost as strings of a harp are plucked. At the points marked by arrows, a dislocation forces several steps into contact, from which one breaks free (see the frame marked 26). The remaining four steps finally coalesce to form nanofacets of both 60° types visible in the image. In this way an external force can nucleate nanofacets.

Grain boundary-induced nucleation. Dislocations induce faceting in a second process that has been observed and documented but remains poorly understood. What happens is that edge dislocations, when organized into low-angle grain boundaries, cause an existing step bunch to nucleate a new $(01\bar{1})$ nanofacet. This occurs for the [100] miscut, despite the fact that the $(01\bar{1})$ facet is poorly oriented, at a large angle to existing steps, unlike the $(\bar{1}10)$ and $(\bar{1}01)$ facets that are more generally preferred for this miscut. Once nucleated, the $(01\bar{1})$ facet then grows, often until it extends fully across the two terraces between neighboring multiple steps. Inevitably this process *increases* the length of the step edge, and also the associated energy cost. As the processes occurs spontaneously and growth continues, we infer that a compensating energy reduction must occur elsewhere. It is possible that the particular facet orientation effectively removes strain energy from the dislocation fields of the low-angle grain boundary, and that this provides the main driving force for the observed process.

The behavior is illustrated by the micrographs of Fig. 6(b). The top figure shows a field with step bunches several steps in height. Below that is the image about 3 h later when the $(01\bar{1})$ nanofacets have formed and ripened, so that the step edges are cut by strong [100] lines; these occur where $(01\bar{1})$ facets cut the (011) surface, and thus become visible in the LEEM image. Below this image are three series of micrographs in which separate facets, each visible in the main image, are tracked as they nucleate and grow. At time 0 (left) a facet (black arrow) nucleates among three edge dislocations (white arrows). Its growth is tracked up to time 570 sec., at which the facet extends across two terraces from the lower dislocation to the middle one. In the second sequence (middle) the nearby grain boundary (white arrows) causes a step bunch to nucleate a triangle of facets which grow to cross a terrace and almost contact two dislocations. In the third and most complicated sequence, a dislocation strain field initially induces nucleation of two facets, one 60° and the other 90°, from which the system evolves to form all three types of {110} nanofacets all clearly oriented with the dislocations of the low-angle grain boundary. It is interesting that precursors of the final facet geometry are often clearly visible on the surface some time *before* the full faceting occupies that particular position. This appears in the LEEM as fluctuating markings on the terraces where the facet will eventually pass, and also as perturbations of neighboring step edges along the track of the growing facet. Clear examples appear in the 664 and 912 images on the right-hand sequence of Fig. 6(c). The precursor phenomena are not understood at present, but probably relate to dislocation structures to which the precursors lead, and to the resulting relaxation of strain fields in the low angle grain boundaries.

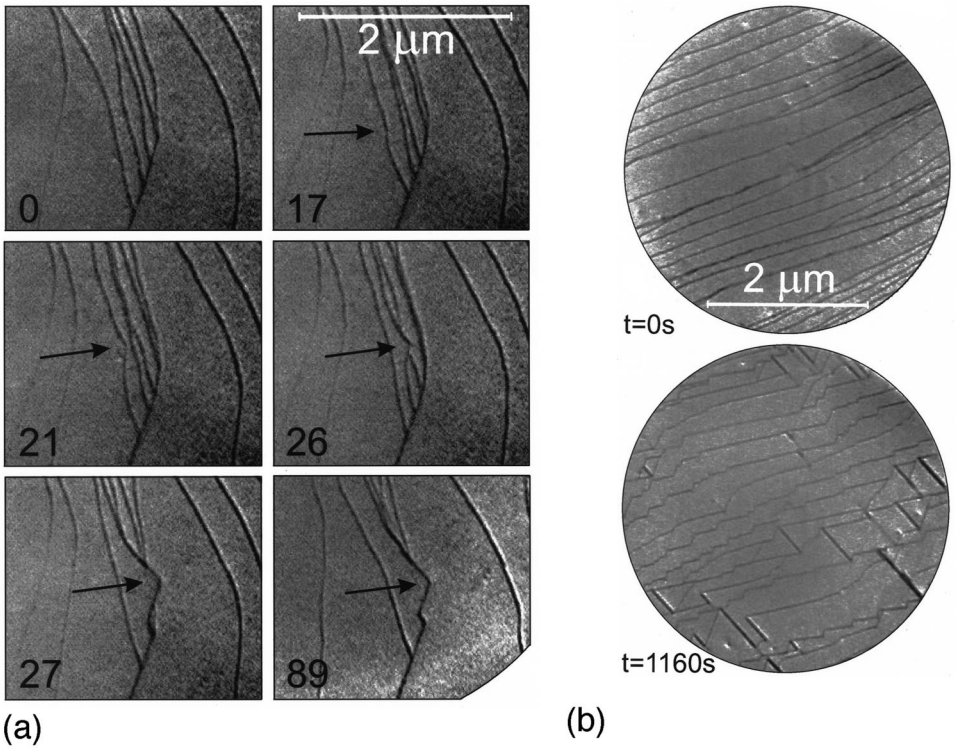

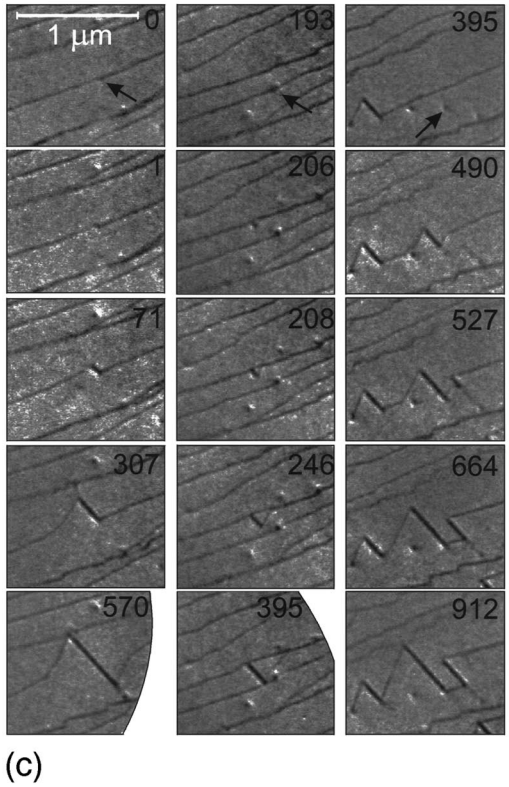

FIG. 6. Nanofacets nucleated near edge dislocations. (a) When a dislocation that intersects the surface (arrows) passes through a field of initially dissociated step edges (image at 0 sec), the dislocation-step interaction forces steps together, and they eventually form two 60° nanofacet (see the image at 89 sec). (b) The upper image shows an initial surface of bunched steps, which after 1160 sec incorporate numerous prominent nanofacets. These include both the expected 60° facets and also anomalous 90° facets whose intersections with (011) lie along [100]. (c) Three sequences are shown in which a 90° facet forms spontaneously from a step bunch in the strain field of a low-angle grain boundary (dislocations marked by arrows). The first sequence (left) is a simple nucleation with subsequent growth of a 90° nanofacet across two terraces, eventually terminating in 60° facets. The second sequence shows three facets nucleating as a triangle from a step bunch, and in the strain field of nearby threading edge dislocations. The third process is more elaborate, including extension to further 90° and 60° facets and other dislocations, and exhibiting precursor markings (see images at 527 and 664 sec) on the surface prior to the final nanofaceting event. The values of E_p in (a), (b), and (c) were 9, 4, and 4 eV, and the temperatures were 1650 K in (a), 1540 K (upper) and 1485 K (lower) in (b), and from 1535 to 1515 K through the sequences in (c).

D. Minimum facet height

A local change of miscut on the surface can cause changes in the faceting. This is particularly striking where the miscut becomes perpendicular to the steps, so that facets are less preferred. In Fig. 7 the upper image is selected to show how steps dissociate from facets, often very slowly, within the temperature range 1500–1650 K. Of special interest is the fact that nanofacets containing different numbers of unit steps dissociate to reveal their actual step contents. In Fig. 7, nanofacets are found in this way to contain three, four, five, etc. steps. It is noteworthy that the two entangled steps on the left, marked by an arrow, do not coalesce to form a true facet along a facet direction, and neither do the two to the right center of the image (arrow). This suggests that for the 60° facets imaged here, a minimum of three step edges is required to form a fully stable facet. Further ex-

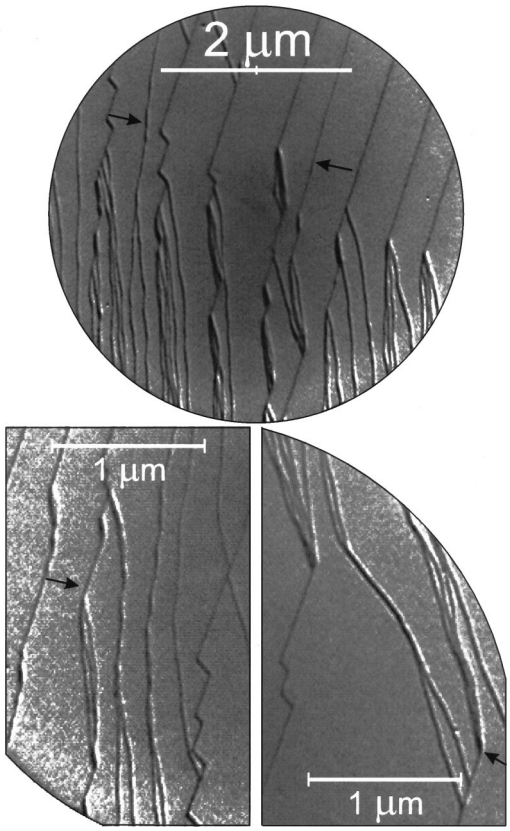

FIG. 7. The upper image shows a region where the local miscut changes and causes nanofacets of various heights to dissociate. Facet heights corresponding to three, four, five, and six steps are visible, but the tangled pairs on the right and left (arrows) fail to adhere accurately to a facet orientation, and thus appear less favorable for facet formation. Image taken at 1585 K with $E_p = 11$ eV. The two images below reveal further details of step interactions and coalescence process for the case of three steps, with $E_p = 9$ eV at $T \sim 1650$ K.

amples verifying that three steps suffice are shown in the lower images, marked by arrows. Each facet has upper and lower edges that bound the facet, and these must contribute positive line energies which destabilize facets more effectively the smaller the facet height. In contrast the $(01\bar{1})$ facets discussed in Sec. III B do appear able to form with just two steps. The latter case differs in two ways from the former. First, the vertical $(01\bar{1})$ facets have an area smaller by a factor $\sqrt{3/2}$ than the 60° $(\bar{1}10)$ facets for the same number of steps, so that their steps bind more strongly; and second, the presence of grain boundary dislocations in the latter case undoubtedly modifies the binding between the step edges. It is possible that the two entangled steps in the lower right image of Fig. 7 form a curved 90° (100) facet, which fails to compete with 60° {110} facets when the height is increased to three steps.

E. Mechanisms for ripening

We have observed the Nb(011) surface after cleaning and during subsequent annealing for extensive periods as the surface structure ripens in the regime where partial or complete faceting occurs. Near 1600 K, the structure changes slowly over the course of hours, and by mechanisms that are relatively subtle. Figure 8(a) contains a sequence of images from a crystal miscut along $[0\bar{1}1]$, which shows one process in which step edges are removed and incorporated into more widely spaced step bunches, with an obvious increase of terrace size and a decrease in free step density. The propeller-like rotation of the step pattern visible at one point in this process is a characteristic feature that recurs frequently in video sequences, and becomes recognizable.

Figure 8(b), taken from an earlier thermal cycling of the same sample, shows steps trapping at low-angle grain boundaries in the process of gradually accumulating to form the large facet of Fig. 4(a), which meanders generally near the [100] direction. The systematic evolution of steps from the terraces to the facet, regardless of temporary pinning at threading edge dislocations, is readily appreciated in the video sequences. Incorporation of existing steps into the facet reduces the net free energy because the free step requires more energy than the same atomic length of vertical {110} surface. However, the detailed mechanism by which the facet attracts the steps still remains to be explained. Step motion requires a net mass transport over the surface to supply or remove the necessary atoms at sites along the step. One possible cause for step migration is that strain fields from the facet cause nearby steps to act as net absorbers or emitters of thermal defects in the form of advacancies and adatoms. A second possibility is that the facet itself boils off thermal defects in nonequilibrium proportions. The behaviors must differ for the 90° inside corner at the foot of the facet and the 90° outside corner at the top of the facet, in order that steps of the same sign be drawn to the facet from both sides.

Figure 8(c) shows images of the more elaborate processes by which the [100] miscut surface evolves toward structures of larger scale. This sample was in the later stages of cleaning after earlier exposure to oxygen. Much of the ripening takes place through the action of screw dislocations, which move through the structure to attach and disconnect various features as the facets develop in height and spacing. In Fig. 8(c) the two upper images compare the surface before and after 250 sec of evolution. It is difficult to comprehend systematic features of the evolution illustrated in the figure, but the surface at the finish of the sequence shown is certainly simplified and on a larger length scale than the starting surface. The set of images shown, with arrows to indicate the motion of screw dislocations, were acquired over the course of 105 sec. The fact that features change in regions remote from the gliding screw dislocations make it difficult to understand the mechanical processes in any detailed way

F. Periodically faceted states

Free step edges are stabilized by the high entropy of the diverse configurations they access, which increases with temperature.[5,6] In contrast, the surface energy of facets is less temperature dependent, and faceting occurs at the lower temperatures. Whereas step edges run perpendicular to the local surface gradient, facets necessarily take crystallographic directions. For this reason the transition from free steps to facets does not always take place at a temperature where the facet and step free energies per unit length are equal. In fact

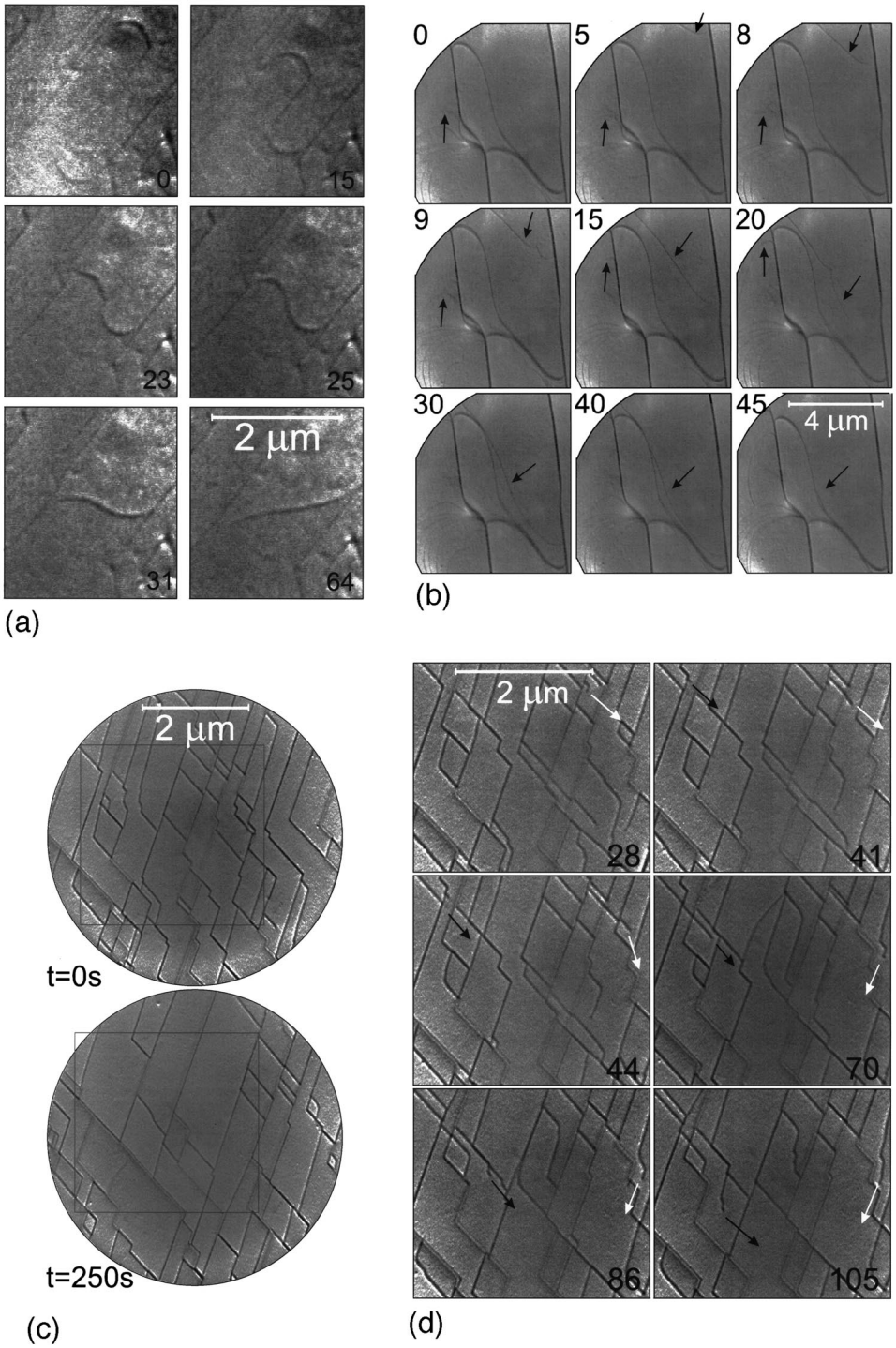

FIG. 8. Ripening mechanisms. (a) A ''propeller'' step process is shown for a crystal miscut along $[0\bar{1}1]$. Excess adatom and advacancy accretion displaces a single step into a step bunch or facet, leaving behind a wider terrace. In sequence (b), nearby step edges are displaced to coalesce with a $(01\bar{1})$ facet on a surface with a weak $[0\bar{1}1]$ miscut. Part (c) charts the ripening of a surface miscut along [100], in which the motion of screw dislocations coarsens the length scale of the structure. The top two images show coarsening that occurs over 250 sec. Details of processes in the frame shown are provided in the lower sequence, where arrows locate individual screw dislocations and indicate their general direction of motion. The values of temperatures and E_p for the three sequences are (a) 1650 K and 9 eV and (b) 1500–1465 K and 4 eV (c) and (d). The temperature rises from 1620 K initially to 1650 K at 250 sec, with $E_p = 4$ eV.

a direct transformation can take place *only* when the steps and facets have the same orientation. Otherwise the facets must have a greater length that the step edges they replace, and dissociated steps therefore remain stable to somewhat lower temperatures.

A separate publication[9] outlines a model which shows that an intermediate phase can occur between the faceted (F) and dissociated step (S) phases. This has been named the periodically faceted phase (P),[9] and is a central component of the phase diagram for nanofaceting, which is the subject matter of Sec. IV. This behavior arises in the regime where the facets have a lower free energy per unit length, but are necessarily longer because they do not follow the optimal surface contour. States in which facets and dissociated steps alternate can have a lower free energy than either steps or facets separately. Sawtooth nanofacets can, on average, follow the miscut contours, but obviously contain a greater length of facet than the length of dissociated steps they replace.

Figure 9(a) shows periodic facets that develop at about 1590 K on *cooling* a Nb(011) surface, miscut close to [100], from an initial condition resembling Fig. 2(a). These structures differ from the sawtooth facets described above, in that facet sections alternate with sections made from dissociated steps, rather than two facet types alternating. The states actually observed here do have alternating sections of facets

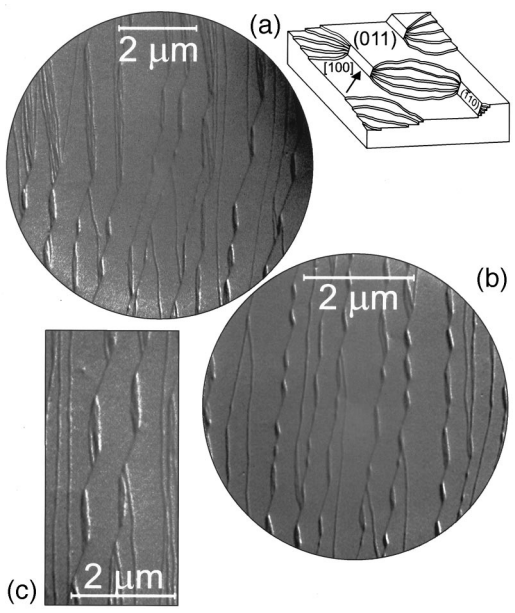

FIG. 9. Periodically nanofaceted states on vicinal Nb(011) miscut along [100] in which nanofacets and dissociated step edges alternate to form a periodic arrangement. (a) Image taken at 1590 K with $E_p = 4$ eV after cooling from a state with steps entirely dissociated. (b) Image obtained at 1600 K with $E_p = 4$ eV after heating from a fully faceted configuration resembling Fig. 4(b). (c) Small region of fairly regular structure from a neighboring region of (a). According to Ref. 9 the periodic faceted states provide the configuration of lowest equilibrium free energy for a range of temperatures for miscut orientations near [100].

and steps, but are not highly periodic. The image of Fig. 9(b) was obtained from a surface resembling Fig. 4(c) upon *heating* to 1600 K. It also shows periodically faceted states in a generally disordered array. It is important that these structures form both on heating and cooling, since this suggests that they may occur in thermal equilibrium. Smaller, more orderly regions do occur, as shown in Fig. 9(c). Like the fully faceted states that occur at lower temperatures (e.g., Fig. 4), the periodic states lack a fundamental length scale, and presumably undergo continued ripening with annealing, in order to decrease the ratio of line energy to surface energy.

IV. PHASE DIAGRAM FOR NANOFACETING

Step edges exhibit a specific energy per unit length when free, and an entropic repulsion when constrained by mutual proximity. While the step spacing becomes larger, as the miscut is reduced at fixed orientation, the free energy change per step edge, as faceting occurs, thus attains a value that is independent of the size of the miscut angle in the limit of infinitesimal miscut. The limiting phase diagram of the surface configuration for small miscut is therefore fixed by miscut azimuth and by the ratio of the step edge energy to the facet energy per unit facet height, which elsewhere is called β.[9] Of course the latter depends on the total facet height, because the line energies where the facet meets the terraces add to the surface energy from the remaining facet area, and the ratio of these components depends on the height. Since this complication does not depend on the miscut, we are free to consider the way the phase diagram for weak miscut depends on the orientation of the miscut and the ratio β of the nanofacet to step energy for a given nanofacet height. No specifically two-dimensional aspects of phase equilibrium influence the notion of a phase diagram for faceting; the entire content is geometrical, relating to the way chemical potential surfaces intersect as functions of the relevant free variables.

Owing to the $(2mm)$ symmetry of the Nb(011) surface (which possesses two orthogonal mirror planes) the Nb(011) surface contains four equivalent quadrants. A second dimension of the phase diagram for faceting is spanned explicitly by β, and hence implicitly by T. Here we construct a speculative phase diagram based on inferences and observations that derive from the results presented above. The phase diagram is given as Fig. 10, with an equilibrium structure shown as a function of T.

In Fig. 10, the portion that falls between the $(\bar{1}10)$ and $(\bar{1}01)$ facet orientations is taken from the discussion of Flynn and Swiech,[9] which assumed that the surface steps have isotropic energies (cf. Fig. 2). It includes a eutectic at which sawtooth facets necessarily transform directly into dissociated steps, marked S. Periodically facetted states, marked P, occur above the eutectic temperature in ''two-phase'' regions with facets equilibrating with dissociated steps that have a different orientation. In this phase diagram, facets play the role of line compounds in metallurgical phase diagrams, and dissociated steps are analogous to liquid or solid solutions that can take a range of concentrations (orientations). Furthermore, since periodically faceted states, as observed, contain dissociations of free steps at angles both larger than and less than π (at the two ends of each facet), it seems certain that much the same type of periodically faceted state must occur, in addition, on the opposite side of the facet orientations (at least when the dissociated steps are indeed isotropic). Thus a further eutectic probably occurs between each 60° facet and the 90° facet, as shown.

Near the $[0\bar{1}1]$ miscut azimuth, the $(01\bar{1})$ facets that form there are shown with an extended phase field. This choice derives from the observation made above from the $(2mm)$ symmetry of the (011) surface, that the facet energy can vary only in second order with the miscut azimuth. While no further results confirm these speculations at present, the proposed second eutectic for 60° facets also requires two phase fields in which 90° facets equilibrate with 60° facets at low temperature, and with dissociated steps at high temperatures. No details of the extent of the latter field are available; widths from zero up remain possible.

The speculative phase diagram for faceting in the limit of small miscut of Nb(011), given in Fig. 10, is consistent with the above discussion. On the other hand, the data are sparse and the regime between $[0\bar{1}1]$ and $[2\bar{1}1]$ is as yet poorly explored. Further measurements are needed before a reliable phase diagram for faceting at small miscut can be fully determined. The Nb films employed here certainly retain some oxygen coverage, and as this can affect step-step interactions we expect that features of the phase diagram for the clean vicinal Nb(011) surface may, accordingly, differ somewhat from those shown. The global phase behavior and its (presumably weak) dependence on facet height and on oxygen coverage nevertheless remains a topic of some considerable interest.

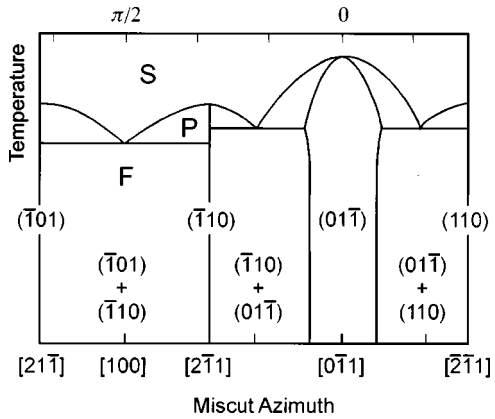

FIG. 10. A speculative phase diagram for nanofacetting of Nb(011) as a function of miscut azimuth for a fixed facet height. The temperature T employed here tracks with a parameter β^{-1}, which measures the ratio of the step-to-facet energy. The facets act like compounds in a metallurgical phase diagram, and the dissociated steps like solutions. The portion of the diagram between the two 60° facet orientations has been calculated by Flynn and Swiech (Ref. 9) for the case of an isotropic step energy. It is expected that the phase diagram changes weakly as the surface ripens and the nanofacets become higher. It may also depend significantly on the oxygen coverage.

V. SUMMARIZING COMMENTS

In this paper we report faceting behavior in which the vicinal Nb(011) surface develops nanofacets with inferred {011} orientations when annealed at temperatures below about 1650 K. The faceting most probably arises from the low surface free energy of the Nb{110} surface, which causes step edges of the vicinal surface to coalesce and form {110} nanofacets. The phenomena on the bcc(011) surface are enriched by the occurrence of three distinct facet orientations, namely, $(01\bar{1})$ which intersects (011) at 90° along [100], and $(\bar{1}10)$ and $(\bar{1}01)$, which intersect (011) at 60° along $[\bar{1}\bar{1}1]$ and $[1\bar{1}1]$, respectively. In the experiments reported here, confined to miscuts of about 0.1°, the former type facets occur for miscut along $[0\bar{1}1]$, and the latter two facets for miscut orientations close to [100].

The phenomena observed include the nucleation of nanofacets directly from dissociated steps and in the perturbing fields of edge dislocations, either singly or in low-angle grain boundaries. The stable phase at sufficiently low temperature comprises long terraces perpendicular to the miscut, terminated laterally either by 90° $(01\bar{1})$ nanofacets or a serrated edge of alternating 60° $(\bar{1}10)$ and $(\bar{1}01)$ nanofacets, for miscuts along $[0\bar{1}1]$ and [100], respectively. A variety of behaviors including sawtooth facet growth, and periodically faceted states occur for the [100] miscut. For both the principal miscuts, mechanisms for a gradual ripening of the structure toward longer length scales are observed.

The phase diagram for faceting as a function of miscut orientation in the limit of small miscut is a further topic investigated here. There is a rich structure in which faceted states, states with dissociated steps, and periodically faceted states all occur. The scale of the structures both in facet length and facet height are subject to ripening with time in order to lower the fraction of energy that edges contribute to the net surface free energy. The scaling of this variation with miscut and facet height is discussed in the Appendix.

ACKNOWLEDGMENTS

This research was supported in part by the Department of Energy Grant No. DEFG02-ER9645439, through the Materials Research Laboratory, where the LEEM is maintained in the Center for Microanalysis of Materials.

APPENDIX: KINETICS OF FACET RIPENING

Here we comment briefly on the way the ripening of faceted nanostructures depends on the length scale of the facets. Suppose the the typical separation of facets is L, and that for a miscut angle θ the facet height is $\sim\theta L$. The line free energy per area L^2, in excess of the {110} facet surface contribution, then varies as ML with M a constant. A doubling of the facet height requires transport of material containing $\sim\theta L^3/\Omega$ atoms, volume Ω, over distances of $\sim L$. The chemical potential gradient is therefore $d\mu/dx \sim(ML/\theta L^3)/L\sim M/\theta L^3$. From the Nernst-Einstein equation the resulting flux per unit area for atoms at density Ω^{-1} is $(D/\Omega kT)d\mu/dx$, and the flow takes place through the surface layer alone, cross section La, with a the layer spacing. We thus find the time constant

$$\frac{1}{N}\frac{dN}{dt}=\frac{1}{\tau}=\frac{\Omega}{\theta L^3}\frac{D}{\Omega kT}\frac{M}{\theta L^3}La.$$

With a scale increase $dL=L$ in a time increment $dt=\tau$, we find

$$\frac{dL}{dt}=\frac{L}{\tau}=\frac{DMa}{\Omega kT}\frac{1}{\theta^2 L^4}.$$

We conclude that the length scale varies with t for various θ as

$$L\sim\left[\frac{MDt}{kT\theta^2}\right]^{1/5}.$$

The experiments described in the text are not sufficiently comprehensive to test this prediction.

*On leave from the Institute of Physics, Acadamy of Sciences of the Czech Republic, Na Slovance 2, Cz-18221 Prague 8, Czech Republic.

[1] F. Liu and M. G. Lagally, Surf. Sci. **386**, 169 (1997); F. M. Ross, J. Tertsoff, and R. M. Tromp, Phys. Rev. Lett. **80**, 984 (1998); M. Kastner and B. Voigtlander, Phys. Rev. Lett. **82**, 2745 (1999); P. Sutter, E. Meteeva, J. S. Sullivan, and M. G. Lagally, Thin Solid Films **336**, 262 (1998).

[2] Island shape and faceting as functions of strain and surface free energy are discussed by I. Daruka, J. Tertsoff, and A. L. Barabasi, Phys. Rev. Lett. **82**, 2753 (1999); R. V. Kutra and L. B. Freund, J. Mech. Phys. Solids **45**, 1835 (1997).

[3] J. C. Heyraud and J. J. Metois, J. Cryst. Growth **50**, 571 (1980); Surf. Sci. **128**, 334 (1983); S. Surnev, P. Coenen, B. Voigtlander, H. P. Bonzel, and P. Wynblatt, Phys. Rev. B **56**, 12 131 (1997); K. Ahrenhold, S. Surnev, P. Coenen, H. P. Bonzel, and P. Wynblatt, Surf. Sci. Lett. **417**, L1160 (1998).

[4] E. D. Williams and N. C. Bartelt, Ultramicroscopy **31**, 36 (1989); M. Wortis, in *Chemistry and Physics of Solid Surfaces*, edited by R. Vanselow and R. Howe (Springer-Verlag, Berlin, 1988), Vol. VII, p. 367.

[5] A. Pimpinelli and J. Villain, *Physics of Crystal Growth* (Cambridge University Press, Cambridge, 1998).

[6] A. Zangwill, *Physics at Surfaces* (Cambridge University Press, Cambridge, 1988).

[7] G. Wulff, Z. Kristallogr. **34**, 449 (1901); for a discussion see e.g., Appendix D of *Physics of Crystal Growth* (Ref. 5).

[8] M. J. Buerger, *Elementary Crystallography* (Wiley, New York, 1963).

[9] C. P. Flynn and W. Swiech, Phys. Rev. Lett. **83**, 3482 (1999).

[10] R. Pantel, M. Bujor, and J. Bardolle, Surf. Sci. **62**, 589 (1977).

[11] R. Franchy, T. U. Bartke, and P. Gassmann, Surf. Sci. **366**, 60 (1996).

[12] L. Vitas, A. V. Ruban, H. L. Skriver, and J. Kollar, Surf. Sci. **411**, 186 (1998).

[13] S. R. Stock, H. Chen, and H. K. Birnbaum, J. Cryst. Growth **84**, 419 (1987).

[14] R. Du, F. Tsui, and C. P. Flynn, Phys. Rev. B **38**, 2941 (1988).

[15] S. M. Durbin, J. A. Cunningham, M. E. Mochel, and C. P. Flynn, J. Phys. F: Met. Phys. **11**, L223 (1981); S. M. Durbin, J. A. Cunningham, and C. P. Flynn, *ibid.* **12**, L75 (1982).

[16] G. Gutenkunst, J. Mayer, and M. Ruhle, Philos. Mag. A **75**, 1329 (1997); **75**, 1357 (1997).

[17] T. Salditt, T. H. Metzger, J. Peisl, C. Morawe, and H. Zabel, in *Evolution of Thin Films and Surface Structure and Morphology*, edited by B. G. Demczyk, E. Garfunkel, B. M. Clemens, E. D. Williams, and J. J. Cuomo, MRS Symposia Proceedings No. 355 (Materials Research Society, Pittsburgh, 1995), p. 269.

[18] J. Mayer, C. P. Flynn, and M. Ruhle, Ultramicroscopy **33**, 51 (1990).

[19] C. P. Flynn and M. B. Salamon, in *Handbook of Physics and Chemistry of Rare Earths*, edited by K. Gschneidner and L. Eyring (Elsevier, Amsterdam, 1996), Vol. 22, p. 1.

[20] G. L. Zhou, S. W. Bonham, and C. P. Flynn, J. Phys.: Condens. Matter **9**, L671 (1997).

[21] M. Huth and C. P. Flynn, J. Appl. Phys. **83**, 7261 (1998).

[22] Here we used substrates from Crystar (Johnson Matthey Co) cut from 2-in. wafers 0.5 mm thick and epipolished on one side.

[23] D. B. McWhan, in *Layered Structures, Epitaxy and Interfaces*, edited by J. M. Gibson and L. R. Dawson, MRS Symposia Proceedings No. 37 (Materials Research Society, Pittsburgh, 1985), p. 493.

[24] G. L. Zhou and C. P. Flynn, Phys. Rev. B **59**, 7860 (1999).

[25] W. Swiech, R. S. Appleton, B. D. Wiemeyer, and C. P. Flynn, Surf. Rev. Lett. **5**, 1221 (1998).

[26] E. Bauer, Rep. Prog. Phys. **57**, 895 (1994).

[27] R. M. Tromp and M. C. Reuter, Ultramicroscopy **36**, 99 (1991).

[28] W. Swiech, M. Mundschau, and C. P. Flynn, Surf. Sci. **437**, 61 (1999).

[29] J. Besold, R. Kuenze, and N. Matz, J. Vac. Sci. Technol. B **12**, 1764 (1994); G. Reiss, L. E. Levine, and D. A. Smith, *ibid.* **11**, 108 (1993).

[30] N. C. Bartelt, J. L. Goldberg, T. L. Einstein, E. D. Williams, J. C. Heyraud, and J. J. Metois, Phys. Rev. B **48**, 15 453 (1993).

[31] See e.g., C. Hammond, *The Basics of Crystallography and Diffraction* (Oxford University Press, Oxford, 1997).

[32] N. C. Bartelt, R. M. Tromp, and E. D. Williams, Phys. Rev. Lett. **73**, 1656 (1994); W. Sweich and E. Bauer, Surf. Sci. **255**, 219 (1991).

[33] O. Hellwig, A. Birkner, and H. Zabel (unpublished).